Sub- and superdiffusive molecular displacement laws in disordered porous media probed by nuclear magnetic resonance

Yujie Li, German Farrher, and Rainer Kimmich
Sektion Kernresonanzspektroskopie, Universität Ulm, 89069 Ulm, Germany
(Received 26 May 2006; published 21 December 2006)

Hydrodynamic dispersion of water flowing through porous glasses with nominal pore sizes in the range 40 to 160 micrometers was studied with the aid of a pulsed gradient nuclear magnetic resonance technique compensating for coherent flow velocities. The crossover from effectively subdiffusive mean square displacement, $\langle Z^2\rangle \propto t^{0.84}$, in the absence of hydrodynamic flow to a superdiffusive, almost ballistic power law, $\langle Z^2\rangle \propto t^{1.95}$, at the highest flow rates was observed. At intermediate flow rates, a gradual conversion between these two limiting power laws occurs. As a function of the Péclet number, the effective dispersion coefficient is in accordance with a power law with an exponent 1.2.

DOI: 10.1103/PhysRevE.74.066309 PACS number(s): 47.56.+r, 82.56.Lz, 05.40.−a

I. INTRODUCTION

The theory of anomalous diffusion is well established. Propagator formalisms have been reported both for sub- and superdiffusive mean squared displacement laws. For a review see Ref. [1]. The purpose of the present study is to demonstrate and examine such laws experimentally.

As outlined in Ref. [2], the origin of anomalous transport properties can be the mutual obstruction of the diffusing particles ("single-file diffusion") and/or the restriction of trajectories to random pore spaces. The latter effectively leads to a kind of trapping hold-up of the particles which consequently may be modeled by a waiting-time distribution. In the following, we will focus on the "trapping" variant of anomalous transport.

Brownian diffusion in random pore networks is subject to a subdiffusive anomaly in the so-called scaling window of the root mean square displacement, $a < \sqrt{\langle Z^2\rangle} < \xi$, where a is the pore dimension and ξ is the correlation length of the pore network [3]. Experimentally this was demonstrated in our previous work with the aid of a random site percolation cluster [4]. On a length scale longer than the correlation length, transport is expected to be normal with some reduced transport coefficient. The present study refers to porous glasses to which a certain degree of randomness can be attributed as well. Apart from Brownian diffusion in the absence of flow, the effect of hydrodynamic advection, that is hydrodynamic dispersion, were examined with the aid of pulsed gradient spin echo techniques [5].

Hydrodynamic dispersion of fluids in porous media due to the combined effect of Brownian diffusion and advection is important in applications such as biological perfusion, chemical reactors and catalysts, soil remediation, and oil recovery. Three mechanisms may lead to dispersion [6]: (a) Taylor dispersion caused by Brownian diffusion of fluid particles across velocity shear; (b) mechanical dispersion, an effect of advection along tortuous paths and streamline bifurcation; and (c) hold-up of fluid particles in the dead ends of pore networks.

In the long time and large displacement limit [7], the probability distribution of the molecule (or tracer) displacements r is expected to be Gaussian with its center moving at the average flow velocity and its second cumulant [8], the mean square displacement, grows linearly in time, i.e., $\langle Z^2\rangle \propto t$. This is in contrast to the situation expected for the scaling window, i.e., at short displacements relative to the correlation length. Particle transport is then subject to anomalous laws [7,9–11]. The probability distribution of r is then non-Gaussian, and there is a tendency to power laws of the form $\langle Z^2\rangle \propto t^{\alpha}$ where $\alpha \neq 1$. If $0 < \alpha < 1$, transport is called "subdiffusive" while $\alpha > 1$ indicates a superdiffusive displacement behavior [1].

Many simulations [11–16] and experiments [11,12,16–22] have been undertaken to examine dispersion in disordered porous media, especially packed beads, both under transient and asymptotic conditions. The influence of the local geometry [14,15,22], mechanical mixing [14], stagnant zones [9,16], and surface relaxation[21] have been studied. However, the crossover from subdiffusive to superdiffusive power laws of the mean squared displacement as expected in the scaling window of disordered media upon the onset of advection was not yet reported.

II. SAMPLES AND EXPERIMENTAL SETUP

The dispersion of water molecules in disordered porous glass was studied under constant flow rates at room temperature. The experimental setup is shown schematically in Fig. 1. The arrows indicate the flow direction.

Two samples were made of porous glasses VitraPor #1 and VitraPor C purchased from ROBU Glasfilter-Geräte GmbH, Germany. The nominal pore sizes are 100–160 μm and 40–60 μm, and the porosities are 0.27–0.28 and 0.33–0.34, respectively. Figure 2 shows typical scanning electron micrographs. The samples used for the dispersion experiments had a cylindrical shape with a diameter of 6 mm and a length of 40 mm. The samples were contained in PCTFE (PolyChloroTriFluoroEthylene) sample holders with connectors for the in- and outflow of water. In order to avoid any bypassing of the water, the sample holders were thermally shrunk on the sample cylinders by heating them first to

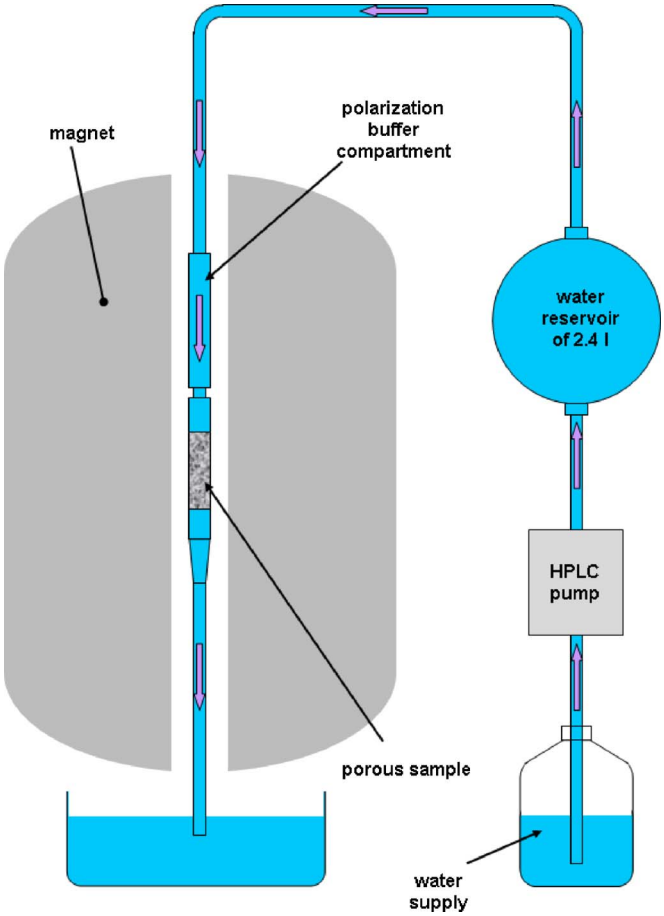

FIG. 1. (Color online) Schematic representation of the setup of the hydrodynamic dispersion experiment in a superconducting NMR magnet. The dimensions of the polarization buffer compartment are 8 mm in diameter and 120 mm in length.

197 °C for about 20 min. While being cold, the sample could be dropped into the sample holder. After thermal equilibration, it was tightly embraced by the PCTFE cylinder and could then no longer be removed without mechanically damaging the container. Before entering the proper sample material, the water passed a buffer compartment in the magnet, where the nuclear spins spent enough time to become polarized prior to the application of the radio frequency (RF) pulse sequence.

The fluid under investigation, distilled water degassed under vacuum for at least 24 h, was pumped by a Lachrom HPLC-pump L-7150 (Hitachi, Ltd., Japan) at flow rates up to 0.9 ml/min through the samples. The flow rates can be varied in steps of 0.1 ml/min. To avoid pulsation artifacts, the pump was buffered by a water reservoir of 2.4 l (see Fig. 1).

The experiments were performed in a Bruker DSX 400 NMR (nuclear magnetic resonance) spectrometer equipped with a vertical 9.4 T magnet. The room temperature bore is 89 mm. A commercial Bruker gradient system with a maximum gradient strength of 1.0 T/m was employed.

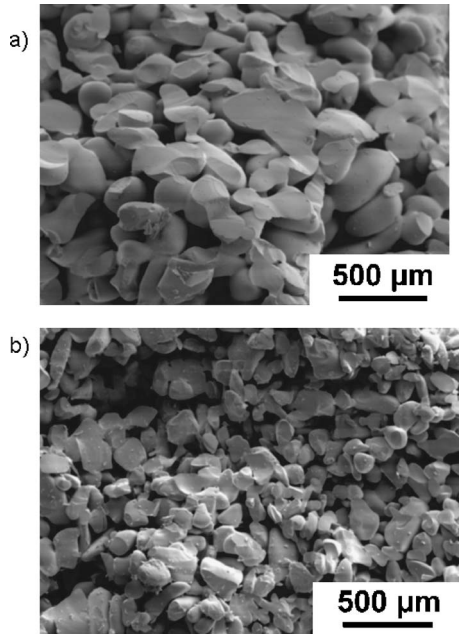

FIG. 2. Scanning electron micrographs of VitraPor #1 (a) and VitraPor C (b) recorded with a Zeiss DSM 962 scanning electron microscope.

III. PULSED GRADIENT NMR MEASURING TECHNIQUE FOR HYDRODYNAMIC DISPERSION WITH COMPENSATION FOR COHERENT VELOCITY EFFECTS

The instantaneous velocity field $\vec{v}$ can be analyzed in two terms according to [6]

$$\vec{v}(t) = \vec{u}(t) + \vec{V}, \tag{1}$$

where $\vec{V} \equiv \lim_{t\to\infty}\langle\vec{v}\rangle$ is the average velocity, and $\vec{u}(t)$ is the fluctuation of the Lagrangian velocity. The principle of the NMR echo attenuation pulse sequences employed in this study is to compensate for the phase shift effect by $\vec{V}$ and to examine the attenuation by $\vec{u}(t)$ [5,23]. Since all position and velocity symbols to be used in this context refer to components along the gradient direction, we will omit the vector symbols in the following for simplicity.

The trajectory of a nucleus may be expressed as follows:

$$r(t) = r_0 + \int_0^t v(t)dt = r_0 + \int_0^t [V + u(t)]dt$$

$$= r_0 + Vt + \int_0^t u(t)dt, \tag{2}$$

where r_0 is the initial position. A field gradient pulse of an arbitrary shape,

$$G = \begin{cases} G(t) & \text{for } 0 \leqslant t \leqslant T, \\ 0 & \text{otherwise}, \end{cases} \tag{3}$$

produces the accumulative phase shift

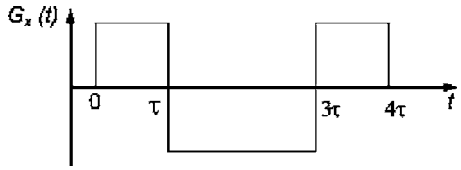

FIG. 3. Field gradient pulse designed for the compensation of phase shifts by position and coherent velocities.

$$\phi(T) = \gamma_n \int_0^T G(t) r(t) dt$$
$$= \gamma_n \left[r_0 \int_0^T G(t) dt + V \int_0^T G(t) t dt + \int_0^T G(t) u(t) dt \right]$$
$$= \phi_0(T) + \phi_1(T) + \phi_2(T), \quad (4)$$

where γ_n is the gyromagnetic ratio of the nucleus. The phase shifts by the position dependent term $\phi_0(T)$ and the coherent-velocity dependent term $\phi_1(T)$ can be compensated by using a bipolar gradient pulse (Fig. 3):

$$G_2(t) = \begin{cases} G_0 & \text{for } 0 \leqslant t \leqslant \tau, \\ -G_0 & \text{for } \tau \leqslant t \leqslant 3\tau, \\ G_0 & \text{for } 3\tau \leqslant t \leqslant 4\tau, \\ 0 & \text{otherwise.} \end{cases} \quad (5)$$

That is, $\phi_0(4\tau)=0$ as well as $\phi_1(4\tau)=0$ after this bipolar gradient pulse. Merely the fluctuation term $\phi_2(4\tau) = \gamma_n G_0[\int_0^\tau u_z(t)dt - \int_\tau^{3\tau} u_z(t)dt + \int_{3\tau}^{4\tau} u_z(t)dt]$ still contributes.

Practically, a combination of 180° RF pulses and unipolar gradient pulses of width δ can be used instead of the bipolar scheme. Figure 4(a) shows such a pulse sequence. A 180° RF pulse effectively inverts the polarity of a previous gradient pulse. The use of two identical gradient pulses with a small gap, τ_m, in between instead of a single, twice as long gradient pulse has a technical reason: It ensures that the gradient amplifier produces identical pulses of well defined "area" $G\delta$. To our experience, a value $\tau_m \approx 4$ ms is sufficient to avoid technical artifacts on this basis. Relative to the relatively long dispersion (or diffusion) time, 2Δ, this interval can certainly be neglected.

Transverse relaxation times in systems like the present ones tend to be very short. That is, echo signals after long intervals Δ are very small for this reason. It is therefore more favorable to use the pulse sequence variant shown in Fig. 4(b). The 180° RF pulses are split into two 90° pulses with a spoiling gradient pulse in between. The 90° RF pulse store half of the magnetization along the z direction parallel to the main magnetic field and read it out again at the end of the interval Δ. In this interval, the magnetization is thus attenuated only by spin-lattice relaxation which is much slower than transverse relaxation. The spoiling gradient pulse spoils all spin coherences in the interval Δ. The use of 90° RF pulse pairs [Fig. 4(b)] instead of 180° RF pulses [Fig. 4(a)] reduces the echo amplitude by a factor of $\frac{1}{4}$ on the one hand, but avoids excessive transverse relaxation losses on the other.

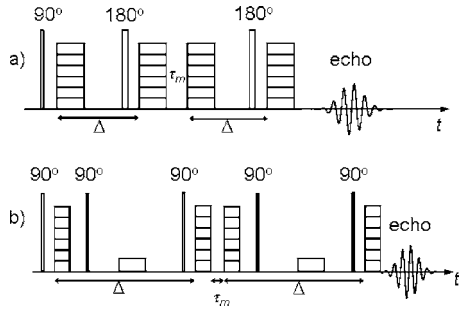

FIG. 4. (a) Coherent velocity compensation RF and field gradient pulse sequence for NMR experiments probing hydrodynamic dispersion. (b) Optimized version avoiding excessive transverse relaxation losses of the signal intensity.

The pulse sequence of the choice thus is the one shown in Fig. 4(b). It compensates for phase shifts by coherent displacements, i.e., by the mean velocity, while incoherent displacements by molecular diffusion and dispersion are encoded in the (identical) intervals $\Delta \gg \tau_m$, and lead to attenuation of the echo amplitude. Note that when we mention the dispersion time in the following, we always mean the combined interval 2Δ.

In the dispersion experiments described in the following, the encoding gradients, G, were incremented in subsequent scans. The echo amplitudes were recorded while all intervals were kept constant. That is, the echo amplitude was measured with the aid of the pulse sequence shown in Fig. 4(b) for given values of the effective dispersion time 2Δ as a function of $2q^2\Delta$ where the wave number is defined by $q = \gamma_n G \delta$. The echo attenuation curves were measured in two experimental series. The "initial" decay, that is the low-wave-number section, was first probed in detail with 32 gradient increments until the echo amplitude decayed to 30–70%. In a second round, the decay to less than 1% was acquired in 64 increments. The dispersion time 2Δ ranged from 36 ms to 450 ms. The evaluation of the attenuation curves will be described below in the context of the results.

We are mainly interested in the *incoherent* contribution to the mean squared displacement along the z direction, $\langle Z^2 \rangle \equiv \langle (z(t) - z(0))^2 \rangle$, where $z(t)$ is the z coordinate of a molecule at time t in a reference frame traveling with the *coherent* contribution by flow. That is, $\langle z \rangle = 0$ relative to this frame. The measuring technique with (coherent) velocity compensation described above provides information on this sort of mean squared displacement. Note that the z axis is the direction in which both the field gradient and the main flow were aligned, so that the longitudinal dispersion is probed (compare Ref. [24]).

IV. RESULTS

Figures 5(a) and 5(b) show typical echo attenuation curves of static and flowing water in VitraPor #1. With flow, there is some tendency to nonexponential decays. This may originate from the pore size distribution and/or the existence of some stagnant parts in the porous medium. Anticipating in this sense that the nonexponentiality is due to a heteroge-

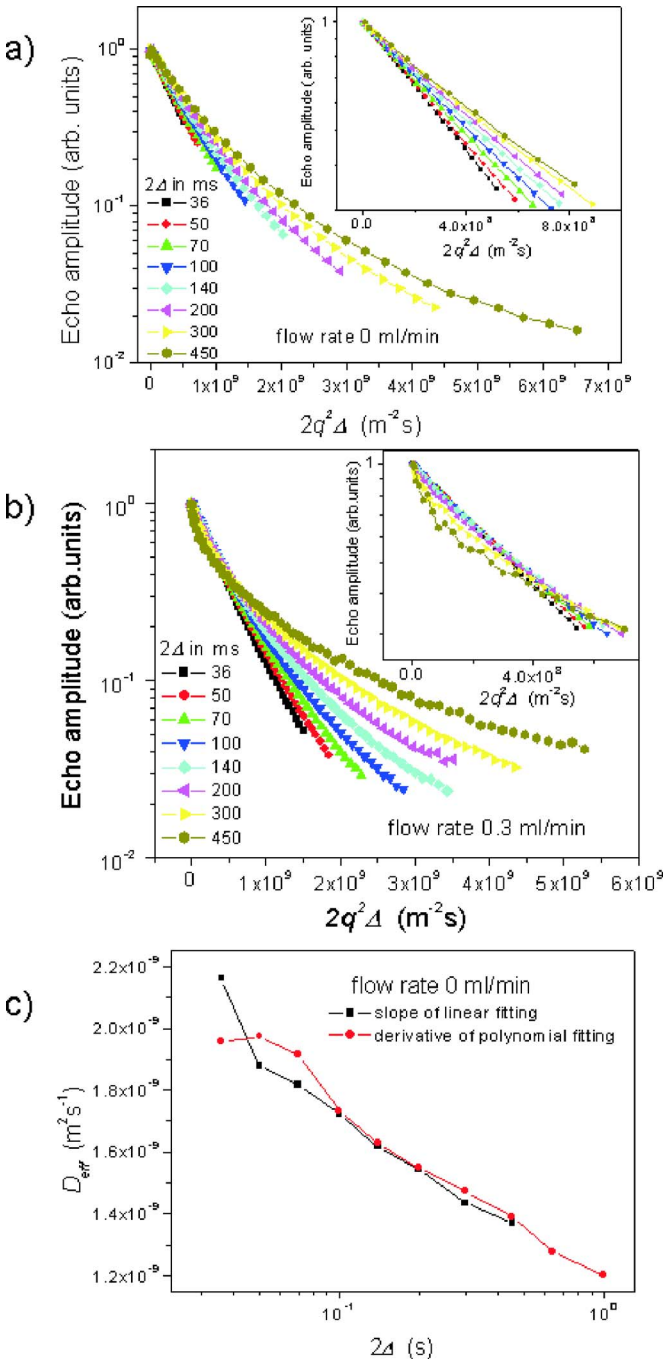

FIG. 5. (Color online) Echo attenuation functions measured with the pulse sequence shown in Fig. 4(b) in the absence of flow (a) and at a flow rate of 0.3 ml/min (b). The curve parameter is the effective dispersion time 2Δ. The insets show the initial, almost monoexponential sections of the decay curves. The effective dispersion coefficient, D_{eff}, was evaluated from the initial slopes or from polynomial fits to the whole curves. A comparison of typical results is shown in (c) and demonstrates the equivalence of the two evaluation protocols.

neous superposition of exponential functions, a mean value of the diffusion or dispersion coefficient can be evaluated from the initial slope of the decay curves, that is in the limit of small abscissa values of $2q^2\Delta$. In this limit, the attenuation function is approached by the proportionality [2]

$$E(q,\Delta)_{q\to 0} \propto \exp(-2q^2 D_{eff}\Delta). \tag{6}$$

The coefficient determined in this way will be called "effective dispersion coefficient," D_{eff}, and tends to be a function of the dispersion time.

The effective dispersion coefficient was evaluated either directly from the initially exponential decay of the attenuation curves or the whole curves were first approached by a linear combination of polynomials from which the slope for $q=0$ was then determined. Both methods led to results in good accordance as demonstrated in Fig. 5(c).

In the absence of flow, D_{eff} decreases with increasing dispersion time. This indicates the influence of the tortuosity of the diffusion pathways increasing with the mean displacements relative to the correlation length. For flow rates between 0–0.2 ml/min, D_{eff} first decreases and then increases with 2Δ. When the flow rate is larger than 0.2 ml/min, D_{eff} increases in the whole dispersion time range probed, 2Δ =36–450 ms. That is, the effective dispersion coefficient is a function of time, $D_{eff}=D_{eff}(t)$.

Anticipating that the displacement propagator can be approached by a Gaussian function (compare Ref. [25] where propagators for sandstone have been evaluated), the mean-square displacement along the gradient direction can be determined according to [2,26]

$$\langle Z^2\rangle \approx 2D_{eff}(t)t, \tag{7}$$

where t is equal to the dispersion time 2Δ in our experiments. If the propagator is not Gaussian, an approximated evaluation from echo attenuation curves is anyway possible in the small-wave number limit as outlined in Ref. [27] on p. 55, for instance. Figures 6(a) and 7(a) show plots of the $\langle Z^2\rangle$ data obtained in this way for different flow rates in the range 0–0.9 ml/min as a function of the dispersion time.

A power law of the form $\langle Z^2\rangle \propto (2\Delta)^{\alpha}$ can be stated in the frame of the experimental accuracy for low and high flow rates. This applies in particular to the flow rates 0, 0.8, and 0.9 ml/min. Obviously a crossover between the subdiffusive limit in the absence of flow to a superdiffusive limit in the presence of strong enough flow occurs. The fitted exponents are $\alpha\approx 0.84$ and $\alpha\approx 1.95$, respectively, for the time window probed in the experiments. The reliability limits of these evaluations are ±0.05. The anomalies of the mean squared displacement power laws are obvious. Interestingly, the same values for the exponent were found in both VitraPor samples in the frame of the experimental error.

The root mean square displacements probed experimentally in VitraPor #1 ranges from 10 to 200 μm. This is the length scale of the pore space topology. That is, the transport properties refer to the scaling window where a power law behavior can be expected. In the absence of flow, transport is governed by molecular diffusion which is obstructed by the confining geometry. The consequence is the subdiffusive mean squared displacement law. Above a flow rate of about 0.7 ml/min, the exponent $\alpha\approx 1.95$ indicates a superdiffusive law approaching the "ballistic" case $\alpha=2$. In this limit, particles are displaced in all directions with the same mean velocity. For hydrodynamic dispersion in disordered porous media, this is the case when pure mechanical mixing is re-

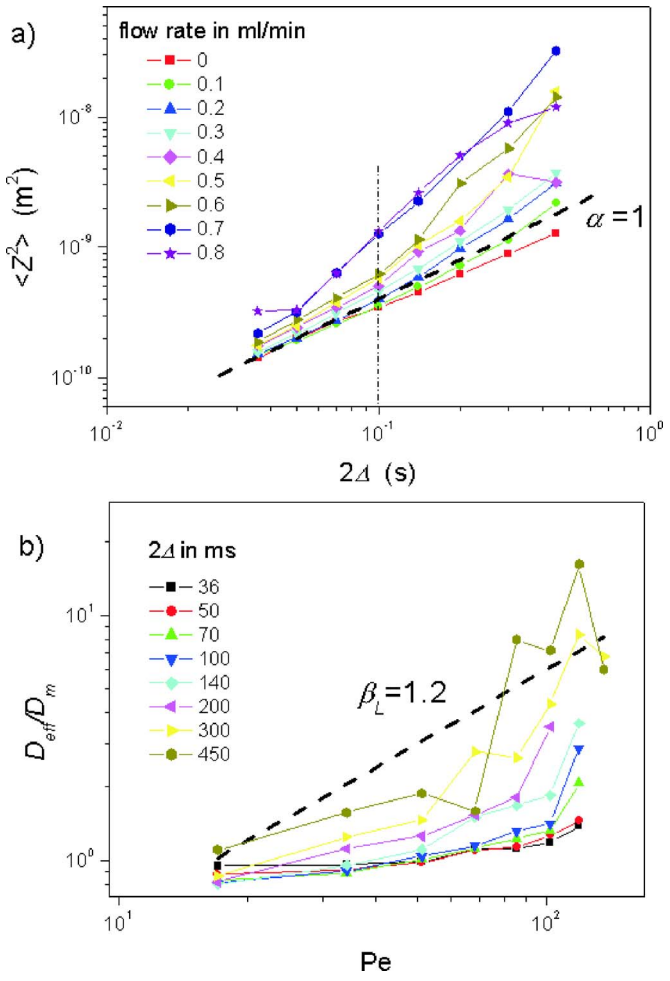

FIG. 6. (Color online) Hydrodynamic dispersion in VitraPor #1 (nominal pore size 100–160 μm). (a) Mean squared displacement, $\langle Z^2 \rangle$, as a function of the effective dispersion time, 2Δ, at different flow rates. The dashed line represents $\langle Z^2 \rangle \propto 2\Delta$. The dash dot line indicates the dispersion time of 100 ms. (b) Dependence of the dimensionless dispersion coefficient D_{eff}/D_m on the Péclet number, Pe, for different dispersion times 2Δ. The dashed line represents the empirical power law $D_{eff}/D_m \propto \mathrm{Pe}^{\beta_L}$ with $\beta_L = 1.2$. The constant c_0 in Eq. (8) is not taken into account here although there is some indication of a plateau at low Péclet numbers and short dispersion times. The thin lines between data points serve as guide for the eye.

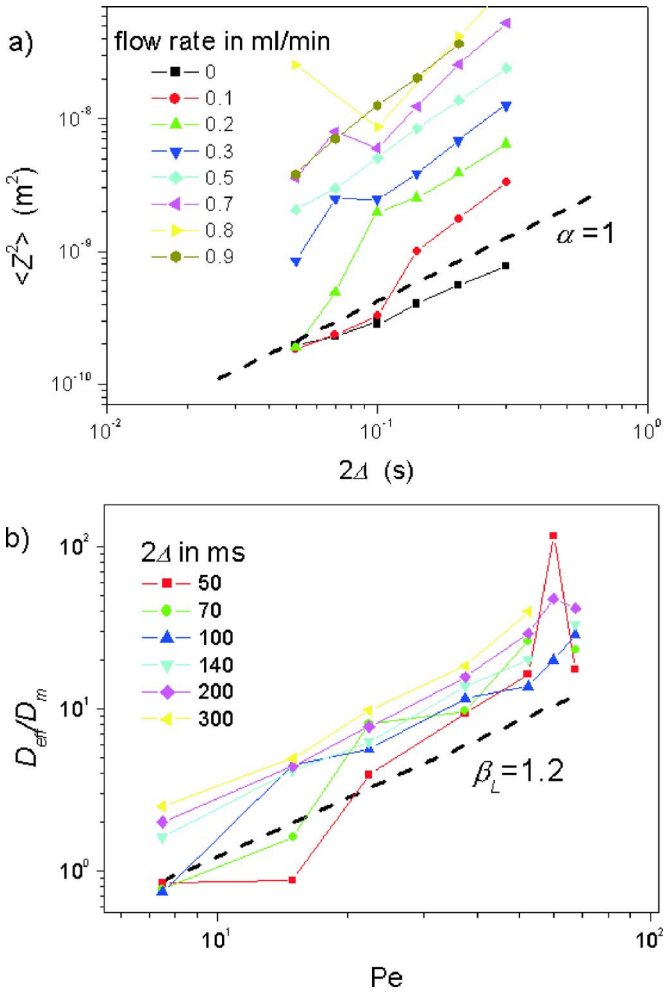

FIG. 7. (Color online) Hydrodynamic dispersion in VitraPor C (nominal pore size 40–60 μm). (a) Mean squared displacement, $\langle Z^2 \rangle$, as a function of the effective dispersion time, 2Δ, at different flow rates. The dashed line represents $\langle Z^2 \rangle \propto 2\Delta$. (b) Dependence of the dimensionless dispersion coefficient D_{eff}/D_m on the Péclet number, Pe, for different dispersion times 2Δ. The dashed line represents the empirical power law $D_{eff}/D_m \propto \mathrm{Pe}^{\beta_L}$ with $\beta_L = 1.2$. Here we have neglected the constant c_0 in Eq. (8) since no plateau at low Péclet numbers shows up. The thin lines between data points serve as guide for the eye.

sponsible under the influence of the local geometry as demonstrated with computer simulations by Duplay and Sen [14].

At relatively low flow rates of 0.1 or 0.2 ml/min, the displacement characteristics tend to be normal or subdiffusive at short dispersion times. However, it appears that a crossover to a superdiffusive displacement law occurs at a dispersion time of about 100 ms [see Fig. 6(a)]. This can be explained by the fact that the root mean squared displacement at such short times is still governed by molecular diffusion whereas flow contributes more efficiently at longer dispersion times.

The dependence of D_{eff}, which is a longitudinal dispersion coefficient (D_L) in our case, on the Péclet number (Pe) is also of interest. It reflects the nature of the mixing process. Fried and Combarnous compiled data for the ratio of the longitudinal dispersion coefficient and the molecular diffusivity, D_L/D_m, as a function of the Péclet number (see Fig. 9.4 in Ref. [7]). At small Péclet numbers, $5 < \mathrm{Pe} < 300$, a law of the form

$$\frac{D_L}{D_m} = c_0 + c_L(\mathrm{Pe})^{\beta_L} \tag{8}$$

is suggested to describe the data [7], where c_0 and c_L are numerical constants. The empirical value of the exponent is $\beta_L \approx 1.2$. In this regime, dispersion is dominated by convection, but the effect of molecular diffusion is not entirely negligible. At larger Péclet numbers, $300 < \mathrm{Pe} < 10^5$, pure me-

chanical dispersion dominates characterized by a linear relation $\frac{D_L}{D_m} \propto \mathrm{Pe}$.

The mean flow velocity in a porous medium is given by

$$V = \frac{f}{A\phi\eta}, \tag{9}$$

where f is the flow rate, A the area of the cross section of the sample, ϕ the porosity, and η the tortuosity. η is defined as D_{1s}/D_m, where D_{1s} is the effective dispersion coefficient in the saturated porous medium for a dispersion time $2\Delta = 1$ s under static conditions. D_m is the molecular diffusivity of bulk water. As usual, the Péclet number is defined as the ratio of coherent and incoherent transport quantities,

$$\mathrm{Pe} = \frac{V\xi}{D_m}. \tag{10}$$

For the analysis of the data presented in the present work, the correlation length ξ is assumed to be much larger than the root mean squared displacement which is of the order of several pore diameters (see Refs. [4,28]). As a typical value we tentatively take three times the pore size. The mean velocity, V, ranges from 9.75×10^{-5} ms^{-1} to 1.2×10^{-3} ms^{-1}. The Péclet number varies accordingly from 8 to 140.

Figures 6(b) and 7(b) show plots of the ratio D_{eff}/D_m versus the Péclet number determined according to Eq. (10) with the dispersion time as a parameter. For comparison, the power law given at Eq. (8) is plotted for an exponent $\beta_L = 1.2$. The data in Fig. 7(b) can be approximated by this law, but a more complicated relationship is suggested by the plot in Fig. 6(b).

V. DISCUSSION AND CONCLUSIONS

Molecular diffusion and hydrodynamic dispersion were studied in random porous glasses. The mean squared displacement and the effective dispersion coefficient were measured noninvasively using a pulsed gradient NMR technique compensating the influence of coherent velocities. The subdiffusive displacement behavior found in the absence of flow turned to clear superdiffusive transport characteristics at the highest flow rates.

In the scaling window, $a < \sqrt{\langle Z^2 \rangle} < \xi$, anomalous power laws for the time dependence were verified as predicted for random media. The exponents range from 0.84 ± 0.05 for the molecular diffusion limit to 1.95 ± 0.05 in the presence of flow. In the latter case, the ballistic flow limit is almost reached. Between these two limits, dispersion gradually evolves from subdiffusion to superdiffusion with increasing flow rates, which demonstrates the competition between molecular diffusion and convection in hydrodynamic dispersion. This is the first time that this sort of crossover was observed in a random medium.

The time scale probed in the present study for diffusion in the absence of flow corresponds to the short-time limit discussed in Ref. [29]. That is, the root mean squared displacement by diffusion is less than the pore dimension, and a slight deviation from the subdiffusive algebraic law anticipated above is expected on this basis. That is

$$\langle Z^2 \rangle \propto t - Ct^{3/2}, \tag{11}$$

where C is a constant, instead of

$$\langle Z^2 \rangle \propto t^{0.84}. \tag{12}$$

However, fits of these laws to the data in Figs. 6(a) and 7(a) are indistinguishable within the experimental error in the experimental time window. Equation (12) may therefore be taken as an approximation effective on the time scale of the experiment.

On the other hand, the time scale is not short enough to reach the limit where the bulk behavior, i.e., normal diffusion dominates. It should also be noted that surface relaxation should not be relevant on the relatively short time scale of our experiments as discussed in Ref. [30].

In a previous work [4], diffusion in a quasi-two-dimensional random-site percolation model object was simulated by solving the ordinary diffusion equation numerically for the corresponding initial and boundary conditions given by spin density mapping experiments. An anomalous time dependence of the mean square displacement $\langle Z^2 \rangle \propto t^{\alpha}$ was obtained with $\alpha \approx 0.8$, while for the present work the experimental value is $\alpha \approx 0.84$ in the algebraic approach for both VitraPor samples within the experimental time window. The mean square displacement can be expressed as follows [4]:

$$\langle Z^2 \rangle \propto t^{2/d_w}, \tag{13}$$

where d_w is the fractal dimension of the random walk. The value suggested by the data in the present work, $d_w \approx 2.38$, is lower than the one reported in Ref. [4], $d_w = 2.87$. The difference is attributed to the different structures. VitraPor is a more or less random porous glass (compare Fig. 2), whereas the percolation cluster in Ref. [4] is designed to have true fractal properties in the scaling window. According to the Alexander/Orbach conjecture [31], the value of d_w is related to the fractal dimension of the structure, d_f, by $d_w = 1.5 d_f$ for Euclidean dimensions $d_E \geqslant 2$. Anticipating fractal properties for VitraPor as well, we find $d_f \approx 1.6$. This value should be taken with some caution, since it first refers to the rather narrow diffusion length scale (one order of magnitude for the mean squared displacement or $10^{-5} - 6 \times 10^{-5}$ m for the root mean squared displacement) probed in the absence of flow, and second is based on the fractal assumption predicting Eq. (13). However, it may serve as an effective characteristic of the porous glass under investigation. Note also, that the displacement length scale under flow conditions probed in Figs. 6(a) and 7(a) was much wider (two and a half orders of magnitude for the mean squared displacement or $10^{-5} - 3 \times 10^{-4}$ m for the root mean squared displacement).

There is an ongoing discussion on theoretical formalisms and predictions for anomalous transport in the literature [1,3,4]. It is clear that these theories can be tested on the basis of the data presented here. However, a condition is that the systems under investigation comply to some universal properties anticipated in the formalisms. The random or even fractal nature of the pore space topology is very crucial in this respect. The fact that a power law behavior was observed in a relatively wide range suggests that this prerequisite is well approached by the VitraPor samples on

the investigated time and length scales, although some singularity showed up for dispersion times around 100 ms for medium flow rates. This possibly corresponds to a structural peculiarity at around 20 μm.

The dependence of the dispersion coefficients on the Péclet number is extensively discussed in Refs. [7,32]. A relation particularly characteristic for dispersion appears to be Eq. (8) suggested for the so-called power-law regime. In the frame of the experimental accuracy, the data presented above are in accordance with this relation. Unfortunately there is no theoretical interpretation of this behavior available in the literature so far (compare Ref. [33]).

ACKNOWLEDGMENTS

We acknowledge support by the Alexander von Humboldt foundation and the Deutsche Forschungsgemeinschaft. We thank Ravinath Kausik for assistance in taking transmission optical microscopic images of the samples, and Carlos Mattea for helpful discussions.

[1] R. Metzler and J. Klafter, Phys. Rep. **339**, 1 (2000).
[2] R. Kimmich, Chem. Phys. **284**, 253 (2002).
[3] R. Orbach, Science **231**, 814 (1986).
[4] A. Klemm, R. Metzler, and R. Kimmich, Phys. Rev. E **65**, 021112 (2002).
[5] R. Kimmich, *NMR Tomography, Diffusometry, Relaxometry* (Springer-Verlag, Berlin, 1997).
[6] P. T. Callaghan, S. L. Codd, and J. D. Seymour, Concepts Magn. Reson. **11**(4), 181 (1999).
[7] M. Sahimi, *Flow and Transport in Porous Media and Fractured Rock: From Classical Methods to Modern Approaches* (VCH Ltd., Berlin, 1995).
[8] U. M. Scheven and P. N. Sen, Phys. Rev. Lett. **89**(25), 254501 (2002).
[9] D. Kandhai, D. Hlushkou, A. G. Hoekstra, P. M. A. Sloot, H. Van As, and U. Tallarek, Phys. Rev. Lett. **88**(23), 234501 (2002).
[10] C. P. Lowe and D. Frenkel, Phys. Rev. Lett. **77**(22), 4552 (1996).
[11] R. A. Damion, K. J. Packer, K. S. Sorbie, and S. R. McDougall, Chem. Eng. Sci. **55**, 5981 (2000).
[12] S. Stapf and K. J. Packer, Phys. Fluids **12**(3), 566 (2000).
[13] L. de Arcangelis, J. Koplik, S. Redner, and D. Wilkinson, Phys. Rev. Lett. **57**(8), 996 (1986).
[14] R. Duplay and P. N. Sen, Phys. Rev. E **70**, 066309 (2004).
[15] R. S. Maier, D. M. Kroll, R. S. Bernard, S. H. Howington, J. F. Peters, and H. T. Davis, Phys. Fluids **15**(12), 3795 (2003).
[16] E. G. Flekkøy, U. Oxaal, J. Feder, and T. Jøssang, Phys. Rev. E **52**(5), 4952 (1995).
[17] A. E. Fischer, B. J. Balcom, E. J. Fordham, T. A. Carpenter, and L. D. Hall, J. Phys. D **28**, 384 (1995).
[18] S. Stapf, Chem. Phys. **284**, 369 (2002).
[19] S. L. Codd and S. A. Altobelli, J. Magn. Reson. **163**, 16 (2003).
[20] M. Deurer, I. Vogeler, A. Khrapitchev, and D. Scotter, J. Environ. Qual. **31**, 487 (2002).
[21] U. M. Scheven, Phys. Rev. E **69**, 021201 (2004).
[22] B. Manz, P. Alexander, and L. F. Gladden, Phys. Fluids **11**(2), 259 (1999).
[23] A. A. Khrapitchev and P. T. Callaghan, Phys. Fluids **15**(9), 2649 (2003).
[24] J. Salles, J.-F. Thovert, R. Delannay, L. Prevors, J.-L. Auriault, and P. M. Adler, Phys. Fluids A **5**, 2348 (1993).
[25] J. J. Tessier, K. J. Packer, J.-F. Thovert, and P. M. Adler, AIChE J. **43**, 1653 (1997).
[26] R. Kimmich, A. Klemm, M. Weber, and J. D. Seymour, Mater. Res. Soc. Symp. Proc. **651**, T2.7.1 (2001).
[27] I. Ardelean and R. Kimmich, Annu. Rep. NMR Spectrosc. **49**, 43 (2003).
[28] O. J. Poole and R. Silbey, J. Phys. Chem. B **104**, 3866 (2000).
[29] P. P. Mitra, P. N. Sen, and L. M. Schwartz, Phys. Rev. B **47**, 8565 (1993).
[30] A. Valfouskaya, P. M. Adler, J.-F. Thovert, and M. Fleury, J. Colloid Interface Sci. **295**, 188 (2006).
[31] S. Alexander and R. Orbach, J. Phys. (Paris), Lett. **43**, L625 (1982).
[32] J. J. Fried and M. A. Combarnous, Adv. Hydrosci. **7**, 169 (1971).
[33] J.-C. Bacri, N. Rakotomalala, and D. Salin, Phys. Rev. Lett. **58**, 2035 (1987).